Hindawi Publishing Corporation
Journal of Nanomaterials
Volume 2016, Article ID 3087491, 9 pages
http://dx.doi.org/10.1155/2016/3087491

Research Article

Adsorption Mechanism of Cu-Doped SnO_2 (110) Surface toward H_2 Dissolved in Power Transformer

Feng Wang, Jingmin Fan, Qiuqin Sun, Qinji Jiang, She Chen, and Wu Zhou

College of Electrical and Information Engineering, Hunan University, Changsha 410082, China

Correspondence should be addressed to Qiuqin Sun; sunqq@hnu.edu.cn

Received 4 September 2016; Accepted 13 November 2016

Academic Editor: Ajayan Vinu

The content of hydrogen is a key quantity in condition assessment and fault diagnosis of power transformer. Based on the density functional theory (DFT), the adsorption mechanism of Cu-doped SnO_2 surface toward H_2 has been systematically studied in this work. Firstly, the relaxation, the bond length, and overlap population of both the pure and Cu-doped SnO_2 are computed. To determine the optimal doping position, the formation energies of four potential sites (i.e., Sn_{5c}, Sn_{6c}, $Sn_{5c\text{-}s}$, and $Sn_{6c\text{-}s}$) are then compared with each other. The adsorption energy and the electronic structure of SnO_2 surface are analysed and discussed in detail. Furthermore, to estimate the partial atomic charges and the electrical conductance, the Mulliken population analysis is also performed. It has been found that the bridge oxygen is the most favourable position. The partial density of states of H_2 after adsorption is broadened and shifted close to the Fermi level. A large amount of charges would be transferred and then released back into its conduction band, leading to the reduction of resistance and the enhancement of sensitivity toward H_2. The results of this work provide references for SnO_2-based sensor design.

1. Introduction

Power transformers are continuously subject to thermal and electrical stresses during the long-term operation. A local overheating or partial discharge would lead to the decomposition of the insulating oil of transformer into gases, including H_2, CH_4, C_2H_4, C_2H_6, C_2H_2, and CO_2 [1]. Compared with other feature gases, the hydrogen is readily separated from dissolved oil and its molecular is the smallest [2–5]. Hence, most of existing online monitoring devices are based on the detection of H_2 [6, 7], and its content is then utilized to assess the condition and diagnose the fault of power transformers.

Presently, a number of sensors have been developed to detect the presence of hydrogen, including the resistive [8–11], the optical fiber [12], the thermoelectric [13], and the surface acoustic wave sensors [14]. Amongst them, the metal oxide semiconductor of SnO_2 is the most employed agent as gas sensor due to its attractive features, such as low cost, small power consumption, and simple structure [15–19]. It has already been applied to air-quality detection, inflammable-gas inspection, environmental monitoring, and so on. However, the pure SnO_2-based gas sensors suffer from the low sensitivity, the slow response, the lack of selectivity, and aging [6, 20–22].

The doping can significantly modify the geometry and the electronic structure of sensor surface. It is one of the most effective methods to improve the gas sensing properties [23, 24]. Various dopants, for example, Pt, Ag, In, Cr, Pd, Ru, and Cu, are often compounded with SnO_2 to detect specific gases. For instance, Jin et al. [25] investigated the sensing properties of Cu-doped SnO_2 of nanofiber structure mainly towards acetone. The results demonstrated that 2.5 wt% Cu exhibited a low optimum operating temperature and displayed the maximum response and selectivity to acetone. The effects of In, Pd, and Pt on CO adsorption have been studied in [26, 27]. Based on the density functional theory (DFT), the interaction between gas and SnO_2 surface on the atomic scale has been studied by means of the first principle calculations. The results indicated that the doping induces some new electronic states in the band gap, leading to the changes of SnO_2 surface properties. In addition, the X-ray diffraction, scanning electron microscopy, and transmission

electron microscopy are increasingly employed to determine the morphology and structure after doping.

Cu is commonly used as a dopant in SnO_2 to improve the sensitivity for detecting hydrogen. It plays an important role in the formation of surface oxygen vacancies in SnO_2. The doping of Cu would inevitably change the bond length, the overlap population, and the electronic structure. Several researchers simply synthesized the Cu-doped SnO_2 sensor using the sol-gel method and then experimentally investigated its gas sensing performance. Despite considerable effort on this subject, the theoretical analysis is still lacking. The mechanism of the doping on the sensitivity toward H_2 is still not well understood and that is the main concern of our work.

The main contribution and the structure of this work are outlined as follows.

(i) The basic structure of SnO_2 surface and the hydrogen adsorption models on potential characteristic atoms have been briefly introduced in Section 2, followed by the description of the computing method.

(ii) Based on the DFT, a series of first principle calculations have been performed on the relaxation, the bond length, and the overlap population of SnO_2 surface. To determine the optimal doping position, the formation energy is then computed, as presented in Section 3.1.

(iii) Section 3.2 is mainly devoted to the adsorption properties. To gain an insight into the interaction between H_2 and SnO_2 surface after doping, the adsorption energy is firstly computed. Then, the electronic structure of SnO_2 surface is analysed. The Mulliken population analysis is performed to estimate the partial atomic charges and the electrical conductance after Cu doping.

(iv) Finally, the conclusion is addressed in Section 4.

2. Models and Computing Method

2.1. Structure of Stoichiometric SnO_2 (110) Supercell. The bulk of SnO_2 has rutile tetragonal structure and the primitive cell of SnO_2 is composed of 2 Sn atoms and 4 O atoms with experimental lattice parameter $a = b = 4.737$ Å, $c = 3.186$ Å. In order to minimize the total energy of the unit cell, the geometry optimization for bulk SnO_2 was performed to relax the ions. The calculated lattice constants are $a = b = 4.699$ Å and $c = 3.164$ Å, which were lower than the experimental values by 0.8 and 0.7%, respectively.

Since the SnO_2 (110) surface is of the lowest energy and the most stable thermodynamic structure among SnO_2 [26–30], it is often regarded as a template in the study of doping. Previous research [29] indicates that 2×1 super cell was suitable to simulate the doping system. When the size of the cell is increased from 2×1 to 2×2, much more computational time would be required. Nevertheless, the formation energy and the charge transfer would not be obviously changed. Hence, it is employed in this work and its structure is illustrated in Figure 1(a).

The surface is cleaved from the optimized bulk of SnO_2, which is represented by a nine-layer slab. Four layers of the slab contain both Sn and O atoms whereas others contain O atoms only. The SnO_2 stoichiometric surface essentially consists of 16 Sn atoms and 32 O atoms, the thickness of which is 13.3 Å, keeping the composition of the primitive cell. There are four kinds of characteristic atoms in the surface, that is, the fivefold coordinated Sn atoms (Sn_{5c}), the sixfold coordinated Sn atom (Sn_{6c}), the bridge oxygen (O_{2c}), and the plane oxygen atom (O_{3c}). The doping, as shown in Figure 1(b), is performed by substituting a Sn atom with Cu. In our work, four potential coordinated Sn atoms are considered. Before the surface relaxation, the atoms on the top four layers are allowed to relax in all directions whereas others are fixed.

2.2. Structure of Cu-Doped SnO_2 (110) Supercell with H_2 Adsorption. Based on the slab model, the adsorptions of H_2 on both the pure and Cu-doped SnO_2 surfaces are studied. The adsorption site perpendicular to the surface is the favoured site from the perspective of energy [31]. Thus, the molecular of H_2 is vertically located on the characteristic atoms and the distance is set to 2 Å, as shown in Figure 2. Referencing to [29], the bond length of free H_2 molecule is set to 0.74 Å and the size of the periodic cell is 10 Å × 10 Å × 10 Å. The geometric structure optimization and adsorption energy calculation are then conducted. During the optimization, the adsorbate and the atoms on the top four layers of the surface are relaxed fully.

2.3. Computing Method. The calculations are performed using the software package CASTEP, which employs a plane-wave basis and periodic super cell method based on the DFT theory. The exchange-correction interactions are treated by local density approximation (LDA) method with the Ceperley-Alder-Perdew-Zunger (CA-PZ) function proposed in [32, 33]. Since LDA method underestimates the band gap [29], LDA+U method has been applied through this paper, where U is set to 3.5 eV to optimize the unit cell of bulk rutile SnO_2. Meanwhile, the ultrasoft pseudo potentials plane-wave basis is employed; the k-points are set to $4 \times 4 \times 1$ to sample Brillouin zone. To guarantee the convergence, the cut-off energy is set to 400 eV. Note that all the calculations are conducted after the optimization, and the vacuum slab is added upon the surface, the thickness of which is set to 16 Å to prevent interactions between periodic images.

3. Results and Discussion

3.1. Properties of Surface

3.1.1. Geometry Structure. To determine the displacement of outmost layer in the relaxed SnO_2 surface relative to their bulk positions, the relaxation of SnO_2 surface is firstly computed, as listed in Table 1.

Clearly, all the outmost atoms have deformed to some extent. The characteristic atoms of O_{2c}, O_{3c}, and Sn_{6c} are shifted along the positive direction of z-axis, and they have moved out of the surface with respect to the bulk termination position by 0.08 Å, 0.10 Å, and 0.20 Å (pure SnO_2 surface), respectively. In contrast, the characteristic atom of Sn_{5c} is

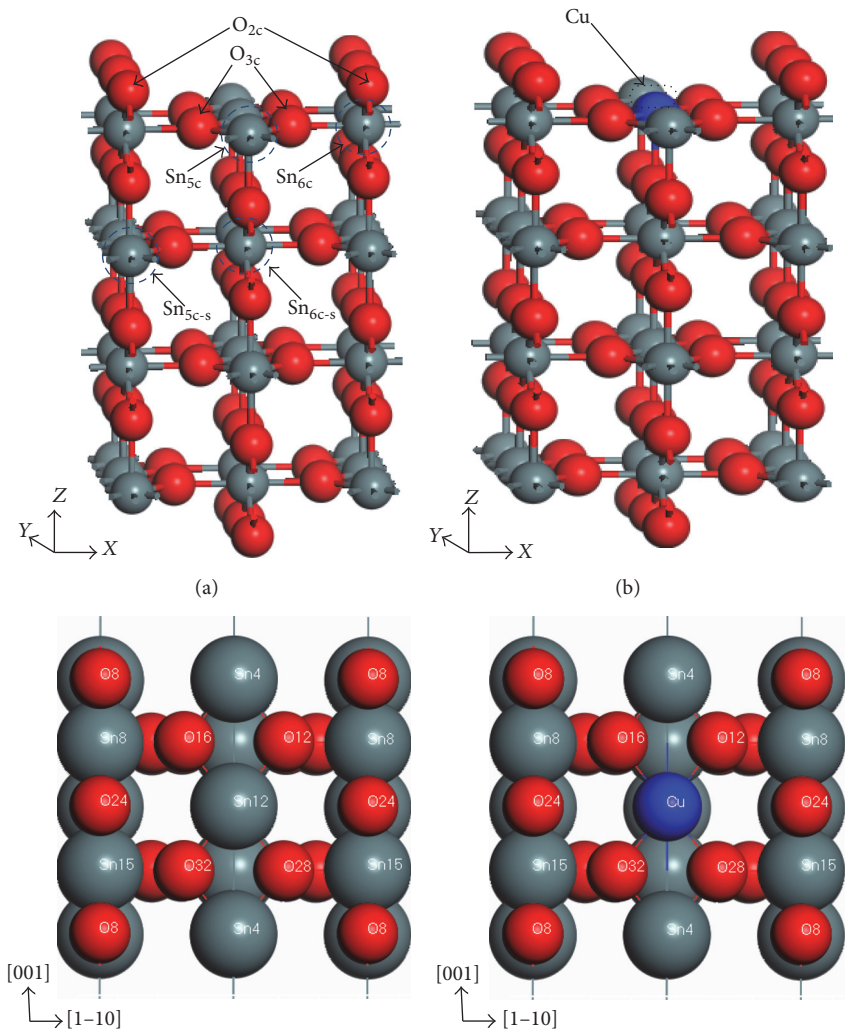

Figure 1: Structure of 2×1 SnO_2 (110) super cell. (a) Undoped SnO_2 (110) surface; (b) Cu-doped SnO_2 (110) surface; (c) top view of undoped SnO_2 (110) surface; (d) top view of Cu-doped SnO_2 (110). Sn_{5c} is substituted by Cu.

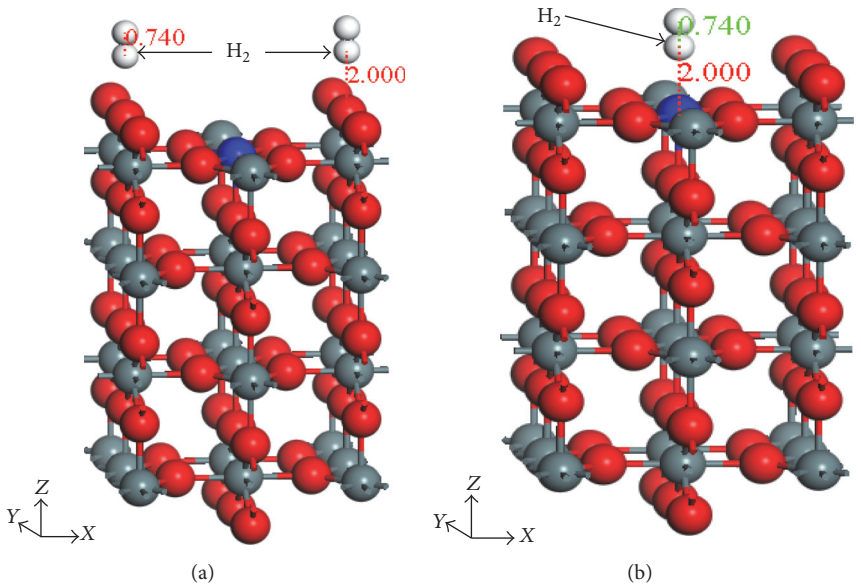

Figure 2: H_2 adsorption on Cu-doped SnO_2 (110) surface. (a) H_2 adsorbed on O_{2c}. (b) H_2 adsorbed on O_{3c}. The distance is set to 2 Å.

Table 1: Displacement of characteristic atoms along (110) direction.

	O_{2c}	O_{3c}	Sn_{5c}	Sn_{6c}	Cu_{5c}
Cu-doped	0.01	0.10	−0.12	0.05	−0.1
Pure	0.08	0.10	−0.11	0.20	—
Reference [34]	0.11	0.20	−0.09	0.23	—
Reference [35]	0.06	0.18	−0.10	0.20	—

Table 2: Bond length and overlap population of pure and Cu-doped SnO_2 surfaces.

	Pure SnO_2 surface		Cu-doped SnO_2 surface	
	BL (Å)	OP	BL (Å)	OP
O12-Sn12	2.013	0.41	—	—
O12-Cu	—	—	2.024	0.32
O12-Sn4	2.013	0.41	2.059	0.38
O8-Sn8	2.099	0.24	2.006	0.43
O12-Sn8	2.099	0.24	2.082	0.29
O24-Sn8	2.013	0.41	1.994	0.45
O8-Sn15	1.968	0.52	2.006	0.43
O24-Sn15	1.968	0.52	1.994	0.45
O28-Sn15	2.099	0.24	2.082	0.29

Notes: the bond length and overlap population of Cu(*Sn12*)-O16, Cu(*Sn12*)-O28, and Cu(*Sn12*)-O32 are the same with Cu(*Sn12*)-O12.

moved along the negative direction, and it relaxes inwards. Cu doping modifies the displacement of characteristic atoms. The most obvious change occurs on Sn_{6c}. The trend and the magnitude of displacement in our work share the same tendency with those presented in [34, 35]. The data provides the essential energies required for the calculation of the formation and the adsorption energies presented in the following sections.

To determine the detailed influence of Cu doping on the atomic structure of SnO_2 surface further, the bond length and overlap population of each characteristic atom in the outmost layer are calculated, as listed in Table 2.

Clearly, Cu doping significantly modifies the local structure of the surface and the most obvious change occurs in the distance between atoms in the top layer. For example, the BL of O8-Sn15 and O24-Sn15 are increased by 0.038 Å and 0.026 Å, respectively, after doping. In particular, the distance between O8 and Sn8 is remarkably reduced from 2.099 Å to 2.006 Å. In terms of the bond length of Cu-O, it is comparable to that of Sn-O. Since the covalent radius of Cu atom (1.17 Å) is smaller than that of Sn atom (1.41 Å), it is larger than that of the other.

Regarding the overlap population (OP), Cu doping causes a decrease in the OP value of O12-Sn4, O24-Sn15, and O8-Sn15, whereas it causes an increment of O8-Sn8, O12-Sn8, O24-Sn8, and O28-Sn15. Correspondingly, the forces between O12-Sn4, O24-Sn15, and O8-Sn15 would be strengthened whereas others are weakened. The modification of the bond length and the overlap population would inevitably lead to the change of the electronic structure of SnO_2 surface.

Table 3: Formation energy of Cu-doped SnO_2 surface (unit, eV).

	Sn_{5c}	Sn_{6c}	$Sn_{5c\text{-}sl}$	$Sn_{6c\text{-}sl}$
Doping formation energy	3.47	4.11	4.67	4.55

The doping of Cu in SnO_2 is achieved through substituting a Sn atom by a Cu atom in the slab model. Four potential sites are considered in our work, that is, Sn_{5c}, Sn_{6c}, $Sn_{5c\text{-}s}$, and $Sn_{6c\text{-}s}$ (see Figure 1). The formation energy is defined as [26]

$$E_{\text{form}} = E_{\text{total}}\,(\text{Cu-doped}) - E_{\text{total}}\,(\text{pure}) + \mu_{\text{Sn}} - \mu_{\text{Cu}}, \quad (1)$$

where E_{total}(Cu-doped) is the total energy of Cu-doped SnO_2 surface supercell, E_{total}(pure) is the total energy of pure SnO_2 surface supercell, and μ_{Sn} and μ_{Cu} are the energy of Sn and Cu atoms in their bulk crystals, respectively. The results of the doping formation energy are listed in Table 3.

Compared with the atoms of $Sn_{5c\text{-}s}$ and $Sn_{6c\text{-}s}$ in the second layer, the doping formation energy is relatively smaller when occurring on the top layer. Correspondingly, the structure is more stable. Among these four coordination atom positions, the formation energy is the smallest when Sn_{5c} is removed by Cu, which indicates the most stable doping form. Hence, the studies on H_2 adsorption presented below are based on this model.

3.1.2. Electronic Structure. The total density of states (TDOS) of Cu-doped SnO_2 surface and the partial density of states (PDOS) of O, Sn, and Cu atoms are depicted in Figures 3 and 4, respectively.

The PDOS of SnO_2 is mainly composed of the valence band and the conduction band. The valance band can be further divided into the lower part and the upper part. It can be seen that the lower part is distributed from −20.5 eV to −15.1 eV, which are mainly from $O2s^2$ electron orbital composition and partly from Sn $5s^2$, $5p^2$ and Cu $3d^{10}$, and $4s^1$ electron orbital composition. In contrast, the upper part is distributed from −9.76 eV to 0.79 eV, which are mainly from $O2p^4$, Sn $5s^2$, $5p^2$, Cu $3d^{10}$, and $4s^1$ electron orbital composition. In terms of the conduction band, it is distributed from 1.68 eV to 9.21 eV, which are mainly from $Sn5s^2$ and $Sn5p^2$ electron orbital composition and partly from $O2s^2$ and $O2p^4$ electron orbital composition.

Compared with pure SnO_2 surface, the valence band is slightly increased after doping. However, the conduction band is drastically changed. The Fermi level, which refers to zero energy, is shifted towards higher energy but the conduction band is moved to lower energy area. The band structure analysis shows that the band gap is narrowed from 0.886 eV to 0.35 eV. Such result agrees well with that reported in [36] but smaller than the experimental value (the band gap of pure SnO_2 is 3.6 eV). The difference is due to the LDA method. It underestimates the binding energy of the d states of Sn, which has a great impact on the band gap [29]. Meanwhile, the electron orbital of Cu $3d^{10}$ was injected into the band gap. The additional electronic states introduced by doping can accelerate the migration of carriers effectively between the bands.

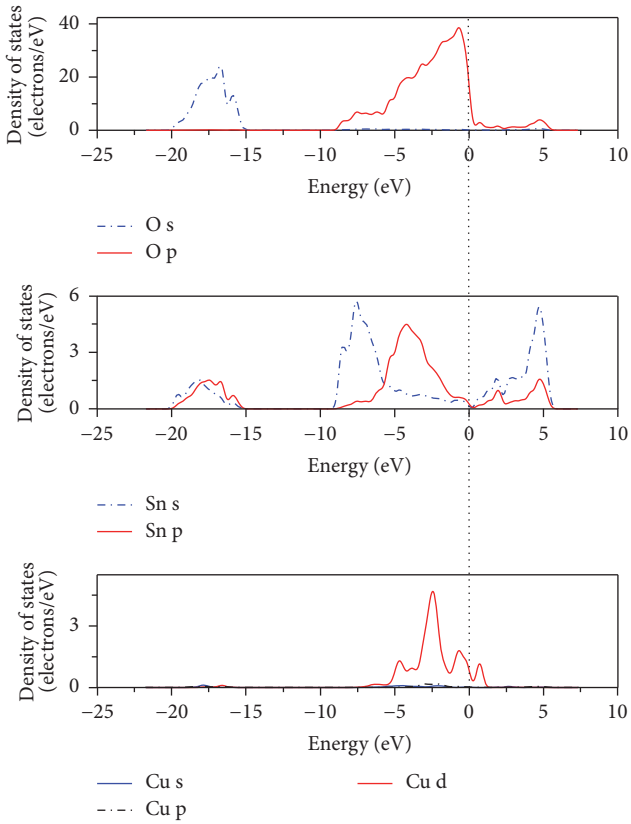

Figure 3: PDOS of Cu-doped SnO_2 surface.

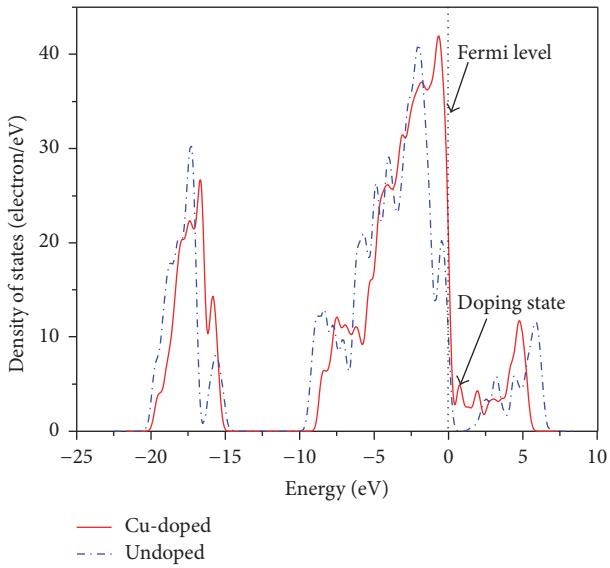

Figure 4: DOS of pure and Cu-doped SnO_2 surface.

3.2. Adsorption Properties

3.2.1. Adsorption Energy. The adsorption energy is a key quantity in evaluating the adhesive property of the system. The energy, which is defined as the reversible energy required to separate an adsorption system into a clean surface and an adsorbed molecular, can be expressed by

$$\Delta E_{ads}(H_2) = E(SnO_2) + E(H_2) - E_{total}(H_2 + SnO_2), \quad (2)$$

where $E(SnO_2)$ and $E(H_2)$ represent the energy of pure SnO_2 surface and free H_2, respectively. $E_{total}(H_2 + SnO_2)$ represent the total energy of adsorption model after geometry optimization. The adsorption energy of both Cu-doped and pure SnO_2 surface is listed in Table 4.

Table 4: Adsorption energy of H_2 adsorbed on Cu-doped and pure SnO_2 surface (unit, eV).

Adsorption energy	O_{2c}	O_{3c}	Sn_{5c}	Sn_{6c}	Cu_{5c}
Pure-SnO_2	0.054	−0.041	−0.017	0.073	—
Cu-SnO_2	0.367	−0.337	−0.299	0.351	0.286

If the adsorption energy is positive, it is an exothermic reaction and the process is spontaneous. Otherwise, the system is energetically instable and the reaction is thermodynamically disfavoured. Generally, the larger the energy, the stronger the gas adsorption.

In terms of pure SnO_2 surface, the adsorption energies of H_2 adsorbed on O_{3c}, Sn_{5c} is negative, which means that O_{3c} and Sn_{5c} are energetically unfavourable adsorption sites. In the case of O_{2c}, Sn_{6c}, and Cu_{5c} adsorption position, ΔE_{ads} is positive and the process is spontaneous. For each kind of adsorption models, the adsorption energy of H_2 on O_{2c} is relatively higher than others, demonstrating that it is the optimal site in the slab model and the probability of adsorption is the largest. This result is consistent with that reported in [37].

Compared with pure SnO_2, the adsorption energy of Cu-doped SnO_2 is greatly increased. The doping of Cu would facilitate the adsorption of H_2. In particular, the adsorption energy on Cu_{5c} is positive, and it means that the H_2 molecular prefers adhesive to the atom. Moreover, Cu becomes an additional adsorption site in the lattice and its presence would further enhance the sensitivity to H_2. It should be pointed out that it is unlikely to determine the exact adsorption energy due to the deviations between the experimental condition and the theoretical model. However, the trend is reliable [31].

3.2.2. Electronic Structure. To gain an insight into the interaction between H_2 and SnO_2 surface, the electronic structure of SnO_2 surface is analysed. Since O_{2c}, Sn_{6c}, and Cu_{5c} are energetically favourable position for H_2 adsorption, this study mainly focuses on these sites. Figure 5 shows the TDOS of SnO_2 surface. It can be found that the profile, the magnitude, and the width have no obvious change after the adsorption. The adsorption does not inject any electronic state into the band gap of the surface, which is similar to CO adsorption on Pd-doped SnO_2 surface [26].

Figures 6, 7, and 8 show the PDOS of free H_2, H_2 adsorbed on pure surface and H_2 adsorbed on Cu-doped surface, respectively. The PDOS of O_{2c}, Sn_{6c}, and Cu_{5c} near Fermi level, ranging from −6 eV to 6 eV, are also included.

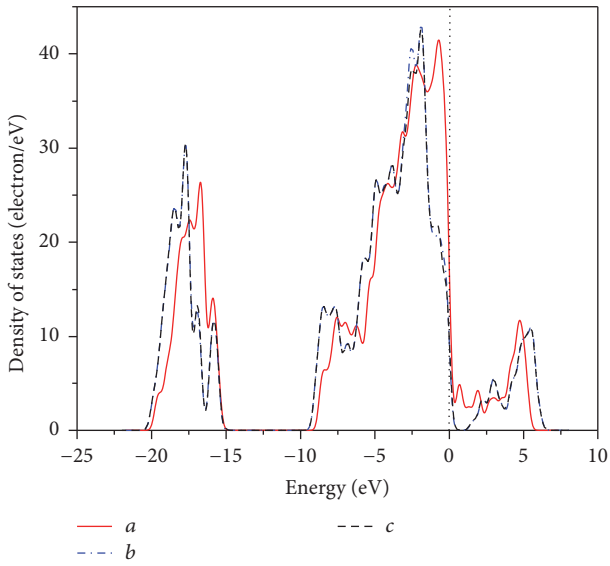

FIGURE 5: TDOS of the SnO_2 surface. (*a*) Pure surface; (*b*) pure surface with H_2 adsorption on O_{2c}; (*c*) Cu-doped surface with H_2 adsorption on O_{2c}.

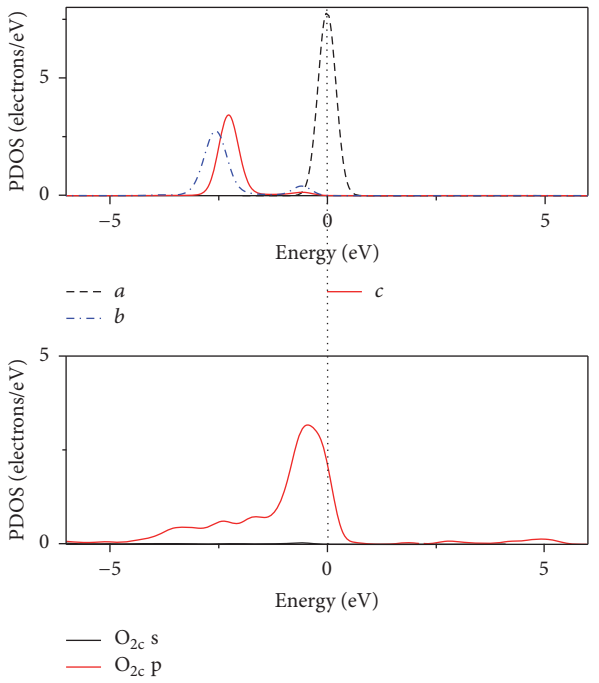

FIGURE 6: PDOS of H_2. (*a*) Free H_2. (*b*) H_2 adsorbed on O_{2c} of pure surface. (*c*) H_2 adsorbed on O_{2c} of Cu-doped surface.

In contrast, there are prominent changes for the DOS of H_2 after adsorption, and the DOS of free H_2 (see the dash line) is located near the Fermi level. While adsorbed on the SnO_2 surface, the DOS of H_2 had a shift towards the lower energy side. Compared with the adsorption on the pure SnO_2 surface, the DOS of H_2 adsorbed on Cu-doped SnO_2 surface is closer to the Fermi level, indicating a greater activity and the facilitation of orbital hybridizations between orbits.

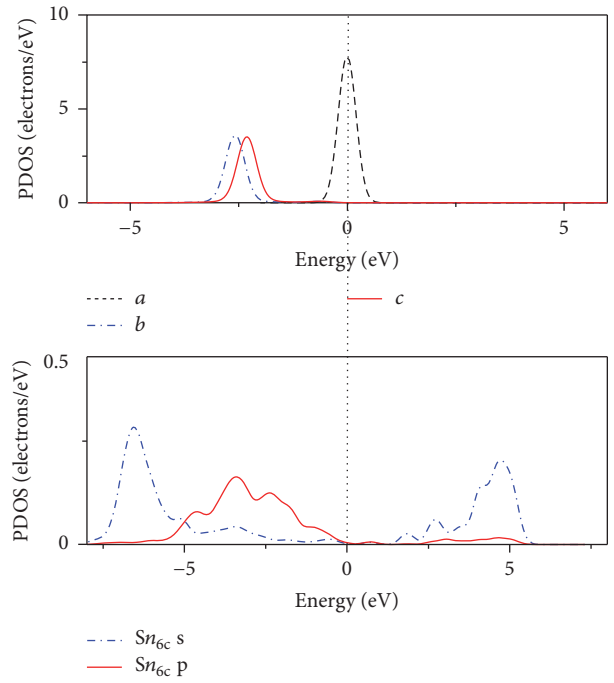

FIGURE 7: PDOS of H_2. (*a*) Free H_2. (*b*) H_2 adsorbed on Sn_{6c} of pure surface. (*c*) H_2 adsorbed on Sn_{6c} of Cu-doped surface.

Amongst the adsorption models, the DOS of H_2 adsorbed on O_{2c} (both pure and Cu-doped SnO_2 surface) and Cu_{5c} (Cu-doped SnO_2 surface) are split into two peaks, which implies that the interaction between the molecular of H_2 and the surface is quite strong in the adsorption process.

From Figures 6 to 8, it can be also found that the DOS of H_2 is broadened, which facilitates the formation of chemical bonds through orbital hybridization. H_2 adsorption on the surface is mainly due to the interaction between the s orbital states of H_2 molecules and the p orbital states of O, s and p orbital states of Sn, and d orbital states of Cu atom. A larger amount of electrons would be transferred in the gas sensing process. Cu doping would enhance the sensitivity to H_2, and the theoretical analysis presented in Section 3.1.2 is further confirmed.

3.2.3. Mulliken Population Analysis. Space charge analysis provides an approach to estimate the partial atomic charges and the electrical conductance. The most commonly used methods are Mulliken and Bader's charge analysis [29]. However, Bader charges sometimes yield too extreme values that suggest much ionic character even in the case of covalent bonds. Mulliken population analysis [17, 26, 27, 37, 38] is employed herein to study the charge transfer between SnO_2 surface and H_2. H_2 adsorption on five potential coordinated sites is considered, as listed in Table 5.

The charges of free H_2 are obtained by summing the charges of two individual atoms. It is clearly that the bond length of H_2 varies significantly after adsorption, from 0.74 Å of free H_2 to 0.84 Å, 086 Å, 0.77 Å, 1.66 Å, and 0.70 Å when adsorbed on O_{2c}, O_{3c}, Sn_{5c}, Sn_{6c}, and Cu_{5c}, respectively. It indicates that H_2 adsorption tends to disassociate. Such

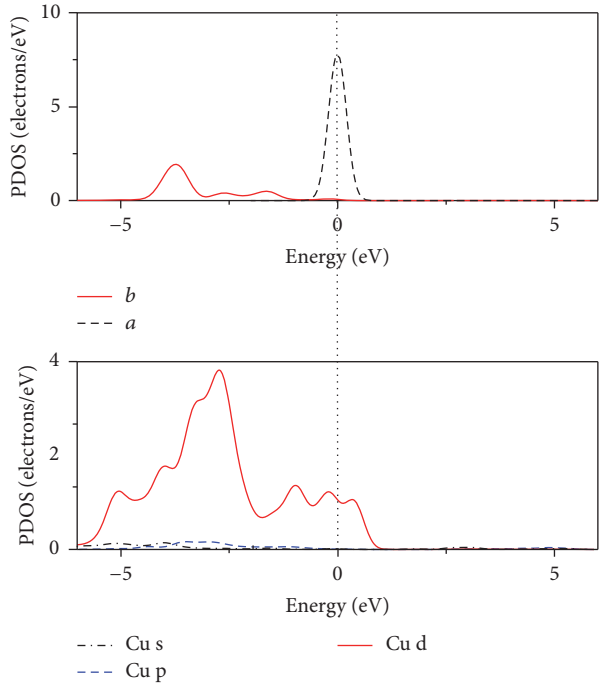

Figure 8: PDOS of H_2. (*a*) Free H_2. (*b*) H_2 adsorbed on Cu_{5c} of Cu-doped surface.

Table 5: Charges of H_2 adsorbed on pure and Cu-doped SnO_2 surface (unit, e).

Adsorption position	O_{2c}	O_{3c}	Sn_{5c}	Sn_{6c}	Cu_{5c}
Pure-SnO_2	−0.17	−0.18	−0.17	−0.17	—
Cu-SnO_2	0	0.31	−0.16	0.79	−0.37

results are similar to H_2 adsorption on pure SnO_2 surface [38] and H_2S adsorption on Cu-doped SnO_2 surface [34].

When H_2 is adsorbed on pure SnO_2 surface, the gas molecule would withdraw charges from the surface. Similar behaviours have also been obtained by Bechthold et al. [18], Menetrey et al. [39], and Sun et al. [40]. Using the first principle method based on DFT, it has been found that the clean SnO_2 surface transfers charges to CO molecule, making it negatively charged.

Regarding Cu-doped SnO_2 surface system, charges are conveyed mainly from H_2 molecular to the surface. The amount of electrons lost by H_2 is as high as 0.79 e, which is much higher than that of pure SnO_2 system. The electrons would be received by the surface and then injected back into the conduction band. Thus, the carrier density of the conduction band would be increased. In addition, both the barrier height of surface depletion layer and the resistance of SnO_2 would decline, leading to the acceleration of the current flowing through the surface and the increment of the output signal of the associated sensors. Consequently, the sensitivity of the sensor towards H_2 would be significantly enhanced. In summary, the doping of Cu would improve the adsorption performance of SnO_2-based sensor toward H_2.

4. Conclusions

In this work, the adsorption mechanism of Cu-doped SnO_2 surface toward H_2 has been studied. The main conclusions are drawn as follows.

(i) The O_{2c} atom is the most favourable adsorption position for hydrogen on both pure and Cu-doped surfaces. The Cu atom provides an additional adsorption site in the lattice after doping, and its presence can contribute to the gas sensing process.

(ii) Since the d states electrons of Cu are injected into the band gap and the conduction band is moved to lower energy area, the band gap of SnO_2 surface is narrowed. The doping of Cu facilitates the migration of carriers between the valence band and the conduction band.

(iii) The PDOS of H_2 after adsorption is broadened and shifted closer to the Fermi level. The interaction between H_2 and the surface is mainly due to the orbital hybridization between the s states of H_2 molecules and the p states of O, s and p states of Sn, and d states of Cu atom.

(iv) After Cu doping, the quantity of electrons transferred from H_2 molecular to SnO_2 surface is substantially increased. The electrons would be captured by the surface and then released back into its conduction band, leading to the reduction of resistance and the enhancement of sensitivity toward H_2.

Competing Interests

The authors declare that there is no conflict of interests regarding the publication of this paper.

Acknowledgments

This work is financially supported by National Natural Science Foundation of China under Grant 51507058. The National Supercomputing Centre, Shenzhen, China, is also acknowledged for providing the computational resources and materials studio (Materials Studio 6.1, MS CASTEP Parallel).

References

[1] R. Liao, H. Zheng, S. Grzybowski, L. Yang, Y. Zhang, and Y. Liao, "An integrated decision-making model for condition assessment of power transformers using fuzzy approach and evidential reasoning," *IEEE Transactions on Power Delivery*, vol. 26, no. 2, pp. 1111–1118, 2011.

[2] Y.-C. Huang and H.-C. Sun, "Dissolved gas analysis of mineral oil for power transformer fault diagnosis using fuzzy logic," *IEEE Transactions on Dielectrics and Electrical Insulation*, vol. 20, no. 3, pp. 974–981, 2013.

[3] B. H. Ward, "A survey of new techniques in insulation monitoring of power transformers," *IEEE Electrical Insulation Magazine*, vol. 17, no. 3, pp. 16–23, 2001.

[4] Z. D. Wang, X. Yi, J. P. Huang, J. V. Hinshaw, and J. Noakhes, "Fault gas generation in natural-ester fluid under localized

thermal faults," *IEEE Electrical Insulation Magazine*, vol. 28, no. 6, pp. 45–56, 2012.

[5] S. A. Khan, M. D. Equbal, and T. Islam, "A comprehensive comparative study of DGA based transformer fault diagnosis using fuzzy logic and ANFIS models," *IEEE Transactions on Dielectrics and Electrical Insulation*, vol. 22, no. 1, pp. 590–596, 2015.

[6] W. Chen, Q. Zhou, F. Wan, and T. Gao, "Gas sensing properties and mechanism of Nano-SnO_2-based sensor for hydrogen and carbon monoxide," *Journal of Nanomaterials*, vol. 2012, Article ID 612420, 9 pages, 2012.

[7] W. Chen, Q. Zhou, T. Gao, X. Su, and F. Wan, "Pd-doped SnO_2-based sensor detecting characteristic fault hydrocarbon gases in transformer oil," *Journal of Nanomaterials*, vol. 2013, Article ID 127345, 9 pages, 2013.

[8] H.-J. Michel, H. Leiste, K. D. Schierbaum, and J. Halbritter, "Adsorbates and their effects on gas sensing properties of sputtered SnO_2 films," *Applied Surface Science*, vol. 126, no. 1-2, pp. 57–64, 1998.

[9] C. Lu and Z. Chen, "High-temperature resistive hydrogen sensor based on thin nanoporous rutile TiO_2 film on anodic aluminum oxide," *Sensors and Actuators B: Chemical*, vol. 140, no. 1, pp. 109–115, 2009.

[10] V. V. Malyshev, A. A. Vasiliev, A. V. Eryshkin et al., "Gas sensitivity of SnO_2 and ZnO thin-film resistive sensors to hydrocarbons, carbon monoxide and hydrogen," *Sensors and Actuators B: Chemical*, vol. 10, no. 1, pp. 11–14, 1992.

[11] N. S. Baik, G. Sakai, N. Miura, and N. Yamazoe, "Hydrothermally treated sol solution of tin oxide for thin-film gas sensor," *Sensors and Actuators, B: Chemical*, vol. 63, no. 1-2, pp. 74–79, 2000.

[12] S. Okazaki, H. Nakagawa, S. Asakura et al., "Sensing characteristics of an optical fiber sensor for hydrogen leak," *Sensors and Actuators, B: Chemical*, vol. 93, no. 1-3, pp. 142–147, 2003.

[13] W. Shin, M. Matsumiya, F. Qiu, N. Izu, and N. Murayama, "Thermoelectric gas sensor for detection of high hydrogen concentration," *Sensors and Actuators B: Chemical*, vol. 97, no. 2-3, pp. 344–347, 2004.

[14] W. P. Jakubik, M. W. Urbańczyk, S. Kochowski, and J. Bodzenta, "Palladium and phthalocyanine bilayer films for hydrogen detection in a surface acoustic wave sensor system," *Sensors and Actuators, B: Chemical*, vol. 96, no. 1-2, pp. 321–328, 2003.

[15] M. Hübner, R. G. Pavelko, N. Barsan, and U. Weimar, "Influence of oxygen backgrounds on hydrogen sensing with SnO_2 nanomaterials," *Sensors and Actuators B: Chemical*, vol. 154, no. 2, pp. 264–269, 2011.

[16] N. Bârsan, M. Hübner, and U. Weimar, "Conduction mechanisms in SnO_2 based polycrystalline thick film gas sensors exposed to CO and H_2 in different oxygen backgrounds," *Sensors and Actuators B: Chemical*, vol. 157, no. 2, pp. 510–517, 2011.

[17] X. Wang, H. Qin, Y. Chen, and J. Hu, "Sensing mechanism of SnO_2 (110) surface to CO: density functional theory calculations," *Journal of Physical Chemistry C*, vol. 118, no. 49, pp. 28548–28561, 2014.

[18] P. Bechthold, M. E. Pronsato, and C. Pistonesi, "DFT study of CO adsorption on Pd-SnO_2(1 1 0) surfaces," *Applied Surface Science*, vol. 347, pp. 291–298, 2015.

[19] Z. Bin, Y. Chenbo, Z. Zili, T. Chunmin, and Y. Liu, "Investigation of the hydrogen response characteristics for sol–gel-derived Pd-doped, Fe-doped and PEG-added SnO_2 nano-thin films," *Sensors and Actuators, B: Chemical*, vol. 178, pp. 418–425, 2013.

[20] L. Boon-Brett, J. Bousek, G. Black et al., "Identifying performance gaps in hydrogen safety sensor technology for automotive and stationary applications," *International Journal of Hydrogen Energy*, vol. 35, no. 1, pp. 373–384, 2010.

[21] C. Lu, Z. Chen, and V. Singh, "Highly hydrogen-sensitive SnO_2 nanoscale-particle films with platinum electrodes," *Sensors and Actuators B: Chemical*, vol. 146, no. 1, pp. 145–153, 2010.

[22] H. Zhang, Z. Li, L. Liu et al., "Enhancement of hydrogen monitoring properties based on Pd–SnO_2 composite nanofibers," *Sensors and Actuators B: Chemical*, vol. 147, no. 1, pp. 111–115, 2010.

[23] A. Stashans, P. Puchaicela, and R. Rivera, "DFT study of chromium-doped SnO_2 materials," *Journal of Materials Science*, vol. 49, no. 7, pp. 2904–2911, 2014.

[24] W. Li, C. Shen, G. Wu et al., "New model for a Pd-Doped SnO_2-based CO gas sensor and catalyst studied by online in-situ x-ray photoelectron spectroscopy," *Journal of Physical Chemistry C*, vol. 115, no. 43, pp. 21258–21263, 2011.

[25] W. X. Jin, S. Y. Ma, Z. Z. Tie et al., "One-step synthesis and highly gas-sensing properties of hierarchical Cu-doped SnO_2 nanoflowers," *Sensors and Actuators, B: Chemical*, vol. 213, pp. 171–180, 2015.

[26] Y. B. Xue and Z. A. Tang, "Density functional study of the interaction of CO with undoped and Pd doped SnO_2(1 1 0) surface," *Sensors and Actuators B: Chemical*, vol. 138, no. 1, pp. 108–112, 2009.

[27] W.-H. Yang, W.-C. Lu, X.-Y. Xue, and Q.-J. Zang, "A theoretical study on CO sensing mechanism of In-doped SnO_2 (110) surface," *Computational and Theoretical Chemistry*, vol. 1069, pp. 119–124, 2015.

[28] T. M. Inerbaev, Y. Kawazoe, and S. Seal, "Theoretical calculations of hydrogen adsorption by SnO_2 (110) surface: effect of doping and calcination," *Journal of Applied Physics*, vol. 107, no. 10, Article ID 104504, 2010.

[29] S. S. Li, Z. S. Lu, Z. X. Yang, and X. L. Chu, "The sensing mechanism of Pt-doped SnO_2 surface toward CO: a first-principle study," *Sensors and Actuators B: Chemical*, vol. 202, pp. 83–92, 2014.

[30] X. Zou, K. Ding, Y. Zhang, and S. Yao, "Acetonitrile adsorption and decomposition on the SnO_2 (110) surface: a first-principles computation," *Theoretical Chemistry Accounts*, vol. 128, no. 1, pp. 63–67, 2011.

[31] W. Zeng, T. Liu, D. Liu, and E. Han, "Hydrogen sensing and mechanism of M-doped SnO_2(M = Cr^{3+}, Cu^{2+} and Pd^{2+}) nanocomposite," *Sensors and Actuators, B: Chemical*, vol. 160, no. 1, pp. 455–462, 2011.

[32] D. M. Ceperley and B. J. Alder, "Ground state of the electron gas by a stochastic method," *Physical Review Letters*, vol. 45, no. 7, pp. 566–569, 1980.

[33] J. P. Perdew and A. Zunger, "Self-interaction correction to density-functional approximations for many-electron systems," *Physical Review B*, vol. 23, no. 10, pp. 5048–5079, 1981.

[34] W. Wei, Y. Dai, and B. Huang, "Role of cu doping in SnO_2 sensing properties toward H_2S," *Journal of Physical Chemistry C*, vol. 115, no. 38, pp. 18597–18602, 2011.

[35] A. V. Bandura, J. D. Kubicki, and J. O. Sofo, "Comparisons of multilayer H_2O adsorption onto the (110) surfaces of α-TiO_2 and SnO_2 as calculated with density functional theory," *Journal of Physical Chemistry B*, vol. 112, no. 37, pp. 11616–11624, 2008.

[36] A. Robina, E. Germán, M. E. Pronsato, A. Juan, I. Matolínová, and V. Matolín, "Electronic structure and bonding of small

Pd clusters on stoichiometric and reduced SnO_2(110) surfaces," *Vacuum*, vol. 106, pp. 86–93, 2014.

[37] W. Zeng, T. Liu, and X. Lei, "Hydrogen sensing properties of low-index surfaces of SnO_2 from first-principles," *Physica B: Condensed Matter*, vol. 405, no. 16, pp. 3458–3462, 2010.

[38] Y. Chen, X. Wang, C. Shi, L. Li, H. Qin, and J. Hu, "Sensing mechanism of SnO_2(1 1 0) surface to H_2: density functional theory calculations," *Sensors and Actuators, B: Chemical*, vol. 220, pp. 279–287, 2015.

[39] M. Menetrey, A. Markovits, and C. Minot, "Reactivity of a reduced metal oxide surface: hydrogen, water and carbon monoxide adsorption on oxygen defective rutile TiO_2(110)," *Surface Science*, vol. 524, no. 1–3, pp. 49–62, 2003.

[40] L. Sun, J. Hu, H. Qin, M. Zhao, and K. Fan, "Influences of Ca doping and oxygen vacancy upon adsorption of CO on the $LaFeO_3$ (010) surface: a first-principles study," *The Journal of Physical Chemistry C*, vol. 115, no. 13, pp. 5593–5598, 2011.